# Parameterization of Turbulent Transport in the Top Meter of the Ocean

JUNSEI KONDO

*Geophysical Institute, Tohoku University, Sendai, Japan*

(Manuscript received 2 December 1975, in revised form 11 May 1976)

ABSTRACT

A hypothesis of hydrodynamic similarity is proposed in respect to both the atmospheric and oceanic boundary layers just above and below their interface. Both layers are combined through an identical geometric surface roughness $h$ which is composed of the high-frequency components of waves. The logarithmic current profiles, hitherto measured in the upper ocean and wind-wave facilities, can be satisfactorily interpreted with the present purely turbulent transport hypothesis. The roughness Reynolds number $hv^*/\nu$ characterizes three surface regimes of the current. The hydrodynamic roughness length and the thermometric and mass transport coefficients are obtained in terms of $hv^*/\nu$. The roughness Reynolds numbers of the oceanic boundary layer are found to be about half those of the atmospheric boundary layer, which implies that the transitions of the oceanic boundary layer to various regimes lag behind those of the atmospheric boundary layer.

## 1. Introduction

A considerable number of studies of the wind in the atmospheric boundary layer above the air-water interface have recently been performed. On the other hand, in the aqueous boundary layer below the interface measurements of wind-induced current have been carried out by only a few workers. However, several findings were made: first, the logarithmic current profiles are seen not only in the laboratory shallow-water channels (Dobroklonskiy and Lesnikov, 1972; Shemdin, 1972; Wu, 1975) but also in the upper ocean and lakes (Kondo *et al.*, 1974); second, the roughness lengths for the current are comparable with those for the wind and have an order of magnitude of 0.01 cm; third, the surface shear stresses obtained from the current logarithmic profile are nearly in agreement with those obtained from the wind profile (Shemdin, 1972; Kondo *et al.*, 1974).

The logarithmic profile must have a nature analogous to that of the profile associated with a turbulent boundary layer above a solid boundary. On the basis of this assumption that the atmospheric boundary layer over a "quasi-rigid" undulating sea surface is aerodynamically similar to the solid boundary, Kondo (1975a) obtained the aerodynamic roughness length $z_0$ and the thermometric and mass-transport coefficients in terms of the roughness Reynolds number of the sea surface. The roughness Reynolds number is very important for estimating the heat and mass transports within the layers immediately adjacent to the rough boundary, since the heat and mass transports are stipulated by this number (Owen and Thomson, 1963). Based on the above, an estimate has been made of the heat and water vapor transports from the sea surface to the atmosphere, and it agrees successfully, within an error of a few percent, with another estimate based on an independent method (Kondo, 1975b).

In spite of wave-induced wind fluctuations having an amplitude of about $A$ [$s^{-1}$] ($A$ being the amplitude of the sea-surface displacement), the mean profile of wind speed always exhibits the logarithmic shape over an undulating sea surface (Kondo *et al.*, 1972). For the aqueous turbulent boundary layer, the author has suggested an idea similar to what was employed for the atmospheric boundary layer.

The present paper emphasizes that previously measured currents are interpreted well by the present hydrodynamic similarity hypothesis involving a purely turbulent fluid without any consideration of a direct contribution from the significant waves. The author does not assert that the instantaneous orbital motion of significant waves has no effect on turbulent transports, but proposes that the wave effect would make a secondary contribution to the current.

## 2. Review of a previous work on currents and the roughness Reynolds number of the sea surface

The solid lines of Fig. 1 are reproductions from the paper by Kondo *et al.* (1974), and indicate the calculated currents which were based on the Stokes mass transport and could be obtained by integrating over the whole frequency range in a wave spectrum (Mitsuyasu, 1971) for a fully developed sea when the friction velocity of wind $u^*=40$ cm $s^{-1}$. For comparison, the measured current profiles are shown by the solid squares for $u^*=40$ cm $s^{-1}$ [obtained by Shemdin (1972) in a 91.5 cm deep wind-wave tank] and by the open circles for $u^*=34$ cm $s^{-1}$ [obtained by Kondo *et al.*

(1974) in the upper layers of the depth of 20 m in the ocean]. From this figure it is clear that the profile measured in the tank has a remarkable similarity with that in the ocean, and that the measured current *shears* are similar to the Stokes current *shears* at the limited narrow range of the distance which depends on the fetch, but the measured and Stokes *velocities* are different.

Regarding the surface Stokes current $V_s$ Kondo *et al.* (1974) obtained

$$V_s=0.0163U_{10\text{ m}}(gF/U_{10\text{ m}}{}^2)^{0.018}, \quad (1)$$

where $U_{10\text{ m}}$ is the wind speed at 10 m under neutral stabilities, $g$ the gravitational acceleration and $F$ the wind fetch. The surface Stokes current is shown by the thin lines in Fig. 4.

If one intends to explain the measured logarithmic current profile using the previously considered view that the drift current is composed of two components (e.g., Wu, 1975), i.e., the wind-drift current and the wave-induced Stokes current, it is necessary to consider very complex mechanisms which vary with wave height and period, fetch, water depth, etc.

Recent observations of the drag in the layers above the air-water interface have suggested that the drag is controlled primarily by high-frequency wave components forming ripples, wavelets and breaking waves. Kondo *et al.* (1973) have found that the representative rms height $h$ of the sea-surface irregularities associated with high-frequency waves (from about 20 to 200 rad $s^{-1}$) is less than the thickness of the atmospheric laminar sublayer under light winds, but increases with wind speed and exceeds the thickness of the laminar sublayer when the wind speed exceeds several meters per second. [The effective wave frequency ranges contributing to surface drag may be different according to interlocked fluids. Between an air-water interface, $h$ is given as $h\approx 0.1+0.009u^*$ for $4\lesssim u^*\lesssim 70$ cm $s^{-1}$, where $h$ is in cm and $u^*$ is in cm $s^{-1}$; it is approximately proportional to the wave height obtainable at a fetch of several meters in a wind-wave facility.]

The above writers have proposed that there are three surface regimes—aerodynamically smooth, transitional and fully rough—classified according to the roughness Reynolds number $hu^*/\nu_a$ ($\nu_a$ being the kinematic viscosity of air), with the values of the Reynolds numbers which delineate the upper limit of the smooth surface regime and the lower limit of the fully rough regime being 5.7 and 67, respectively. It is natural to consider that these numbers would differ according to the range of frequencies in the wave spectrum. The present study has employed the wave frequency range from about 20 to 200 rad $s^{-1}$.

## 3. Application of the hypothesis to the oceanic boundary layer

It is generally accepted that some fraction of the momentum communicated between the atmosphere and the ocean appears first as wave momentum which is lost by breaking and generates small-scale turbulence very near the surface which decays and gradually diffuses downward. [This fraction of the wave momentum amounts to about 3–10% of the total momentum transport (e.g., Imasato and Kunishi, 1971; Taira, 1972; Toba, 1972).] Thus, this small-scale turbulence near the surface must be reflected in the hydrodynamic roughness value of the aqueous boundary layer as well as the roughness value of the atmospheric boundary layer. The other fraction of the momentum transported from the air into the water first generates the surface current which forms the mean velocity gradient and gradually extends downward. Far from the surface, when steady state is attained, the turbulent field in the aqueous layer will be maintained by the mean velocity gradient just as it is in the air. The above is the physical view of the present similarity hypothesis.

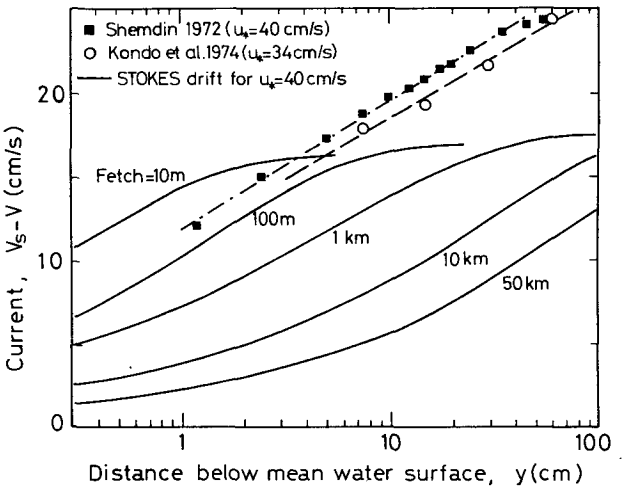


FIG. 1. Stokes current distributions with respect to the moving surface at wind fetches of 10 m, 100 m, 1 km, 10 km and 50 km for $u^*=40$ cm $s^{-1}$.

In the horizontally uniform, aqueous boundary layer we have proposed a hydrodynamic similarity hypothesis which assumes current properties to be described by only the roughness Reynolds number of the interface. If we consider that the geometric roughness lengths of the air-water interface as seen from the wind are identical with those seen from the current, the hydrodynamic roughness length $y_0$ (in terms of $hv^*/\nu$) may be given by the same functional form as that for $z_0$ in terms of $hu^*/\nu_a$, where $v^*=(\tau/\rho)^{\frac{1}{2}}$ is the friction velocity of current, $\tau$ the shearing stress, and $\nu$ and $\rho$ the kinematic viscosity and the density of water, respectively. The generalized resistances for the transports of momentum, heat and mass may be defined, respectively, by

$$f(y)=(V_s-V)/v^*, \quad (2)$$

$$r_T(y)=c\rho v^*(T_s-T)/H, \quad (3)$$

$$r_C(y)=v^*(C_s-C)/M, \quad (4)$$

where $y$ is the depth from the water surface, $V$ the current, $T$ the temperature, $C$ the mass concentration per unit volume, $H$ the turbulent heat flux, $M$ the mass transports, $c$ the isobaric specific heat of water, and the subscript $s$ refers to the surface value. Here we consider sea water to be a substance of comparatively slow chemical reaction.

In the absence of buoyancy effects on transports (see Appendix), that is, when logarithmic profiles are assumed, the resistances are given by

$$f(y)=k^{-1}\ln(y/y_0), \tag{5}$$

$$r_T(y)=k^{-1}\ln(y/y_T)=B_T^{-1}+f(y), \tag{6}$$

$$r_C(y)=k^{-1}\ln(y/y_C)=B_C^{-1}+f(y), \tag{7}$$

for $y_0$, $y_T$, $y_C \ll y \lesssim y_1$, provided no absorbing radiation penetrates the aqueous boundary layer. Here $y_1$ is the thickness of the constant flux layer; $B_T$ and $B_C$ are called the sublayer Stanton and sublayer mass-Stanton numbers, respectively; $y_T$ and $y_C$ are defined as the parameters to which the logarithmic profiles are extrapolated at $T=T_s$ and $C=C_s$, respectively, and are analogous to the hydrodynamic roughness length $y_0$; and $k=0.4$ is the von Kármán constant. In the above equations, an infinitesimal temperature change resulting directly from emitted thermal radiation within the upper micron of depth is neglected (McAlister and McLeish, 1969), and an equality is assumed for eddy diffusivities of momentum, heat and mass transports.

With the aid of a similar process which was applied to the atmospheric boundary layer (Kondo, 1975a), the hydrodynamic roughness length and transport coefficients for the three flow regimes can be obtained as described in the following subsections.

### a. *Smooth regime* ($hv^*/\nu \lesssim 5.7$)

While the present classification of three flow regimes is somewhat arbitrary, it is useful to present the current characteristics in this way. Recognizing a laminar sublayer immediately below the air-water interface, it follows that

$$B_C^{-1}=\lambda(\nu/D)^{\frac{1}{2}}+k^{-1}\ln[(\nu/D)^{\frac{1}{2}}\beta/\lambda], \tag{8}$$

$$B_T^{-1}=\lambda(\nu/\alpha)^{\frac{1}{2}}+k^{-1}\ln[(\nu/\alpha)^{\frac{1}{2}}\beta/\lambda], \tag{9}$$

$$\beta=y_0v^*/\nu, \tag{10}$$

where $\lambda$ is a numerical constant, $D$ the molecular diffusivity of mass, and $\alpha$ the thermometric diffusivity of water.

It is natural to consider that the laminar sublayer does not have a sharp outer boundary, but passes smoothly into the next region of laminar-turbulent flow, and thereafter into the logarithmic-profile region of purely turbulent flow; in this paper the thickness of the laminar sublayer is defined as the depth at which the extrapolated logarithmic profile intersects the linear velocity profile for the laminar flow immediately adjacent to the boundary.

It is well known that the thickness of the laminar sublayer for the velocity profile and that for the temperature profile are given, in a sense of the above definition, as follows (Schlichting, 1968):

$$\delta_V=\lambda\nu/v^*, \tag{11}$$

$$\delta_T=\delta_V(\nu/\alpha)^{-\frac{1}{2}}. \tag{12}$$

From a restriction that requires the stress to be continuous at the border between the linear-profile layer and the logarithmic-profile layer, we obtain

$$\lambda=k^{-1}\ln(\lambda/\beta), \tag{13}$$

yielding a value of $\lambda$ which decreases with increasing $\beta$ for a range of $\beta<0.91$. The value of $\lambda=11.6$ at $\beta=\frac{1}{9}$ corresponds to smooth regimes (Schlichting, 1968) and thus it follows from (10) that

$$y_0=\nu/9v^*. \tag{14}$$

### b. *Transition regime* ($5.7 \lesssim hv^*/\nu \lesssim 67$)

The hydrodynamic similarity hypothesis implies that the functional form of $y_0$ in terms of $hv^*/\nu$ is the same as that of $z_0$ in terms of $hu^*/\nu_a$. The values of $B_C^{-1}$, $B_T^{-1}$, $\delta_V$ and $\delta_T$ can be obtained from Eqs. (8), (9), (11) and (12) by using the variable $\lambda$ which depends on $hv^*/\nu$ (or $\beta=y_0v^*/\nu$), instead of the constant $\lambda=11.6$ for the smooth regime. The decreasing value of $\lambda$ with increasing $\beta$ means that the effective thickness of the laminar sublayer is thinner than that predicted from (11) with a constant value of $\lambda=11.6$. Such a thinner sublayer is supported by the experimental evidence of McLeish and Putland (1975).

[In the present study we need a relationship between $h$ and $v^*$. To do so we use the value of $h$ now given in terms of $u^*$ (Section 2) and the ratio of $v^*/u^*$ which will be shown later.]

Values of $B_C^{-1}$, $B_T^{-1}$, $\delta_V$ and $\delta_T$ can be estimated for the range $5.7 \lesssim hv^*/\nu \lesssim 20$, whereas for the range $20 \lesssim hv^*/\nu \lesssim 67$ the values of $B_C^{-1}$ and $B_T^{-1}$ are obtained by extrapolating their functional forms at the following fully rough regime.

### c. *Fully rough regime* ($67 \lesssim hv^*/\nu$)

For this regime Kondo (1975a) has suggested that

$$h/y_0=15. \tag{15}$$

From the results by Owen and Thomson (1963), Yaglom and Kader (1974) and Brutsaert (1975), together with a personal suggestion by Kondo, we find that

$$B_C^{-1}=b_1(2hv^*/\nu)^p[(\nu/D)^q-b_2]+b_3, \tag{16}$$

$$B_T^{-1}=b_1(2hv^*/\nu)^p[(\nu/\alpha)^q-b_2]+b_3, \tag{17}$$

where $b_1$, $p$, $q$, $b_2$ and $b_3$ are numerical constants whose values have been given as follows: (Owen and Thomson) $b_1=0.52$, $p=0.45$, $q=0.8$, $b_2=b_3=0$; (Yaglom and Kader) $b_1=0.55$, $p=\frac{1}{2}$, $q=\frac{2}{3}$, $b_2=0.2$, $b_3=9.5$ (for $\nu \gtrsim \alpha$, $D$); (Brutsaert) $b_1=3.1$, $p=\frac{1}{4}$, $q=\frac{1}{2}$, $b_2=b_3=0$. In the above equations the numeral 2 multiplying $hv^*/\nu$ expresses the conversion ratio of the equivalent sand roughness length ($=30y_0$) of Nikuradse's experiments to the representative rms height of the sea surface irregularities associated with the high-frequency wave components.

According to the recent paper by Toba *et al.* (1975) certain skin flows on the windward face of the wave crest (revealed in current visualization photographs) accompany large current shear at the water surface converging on the leeward face of the wave crest, creating downward flow and conspicuous turbulent structure. Thus, such turbulent nature must be implicitly reflected in the trend of the present hydrodynamic roughness value $y_0$. For fully rough regimes the top-most layers must be accompanied by both skin and turbulent flows, and as a consequence the laminar layer cannot be identified. We also consider that the logarithmic profile may be applicable to the depth $y \gg y_0$.

## 4. Results and discussion

From Eqs. (8)–(17) the hydrodynamic properties can be obtained in terms of $hv^*/\nu$ (or $v^*$) for all current regimes. The physical constants used are $\nu=0.01$ cm$^2$ s$^{-1}$, $\nu/\alpha=7.1$ and $\nu/D=820$ (for NaCl), 620 (for $N_2$) and 500 (for $O_2$). In Fig. 2 the roughness Reynolds number $hv^*/\nu$ for the current is taken as the abscissa. For reference the scale of the roughness Reynolds number $hu^*/\nu_a$, as seen from the wind, and another scale of the wind speed at a height of 10 m under neutral stabilities are shown below the scale of $hv^*/\nu$. The relationship between $U_{10\,\mathrm{m}}$ and $hu^*/\nu_a$ is referred to by Kondo (1975a). Since both $\tau_a=\rho_a u^{*2}$ and $\tau=\rho v^{*2}$ are of the same magnitude within an error of about $\pm 10\%$, it is assumed that $v^*=(\rho_a/\rho)^{\frac{1}{2}}u^*$ (Shemdin, 1972; Kondo *et al.*, 1974), where $\rho_a$ is the air density. This relation implies that we neglect any stress supported by waves. Accordingly, the roughness Reynolds number of the current may be given in terms of the roughness Reynolds number of the wind by

$$\frac{hv^*}{\nu}=\frac{\nu_a}{\nu}\left(\frac{\rho_a}{\rho}\right)^{\frac{1}{2}}\frac{hu^*}{\nu_a}\approx\frac{1}{2}\frac{hu^*}{\nu_a}, \tag{18}$$

which means that $hv^*/\nu \approx 4$ when $hu^*/\nu_a=8$, and that $hv^*/\nu \approx 50$ when $hu^*/\nu_a=100$. The former, for example, implies that the aqueous boundary layer may be treated as a smooth surface while the atmospheric boundary layer may be in a transition regime. Referring to the abscissas, the critical roughness Reynolds numbers previously introduced, 5.7 and 67, takes place at

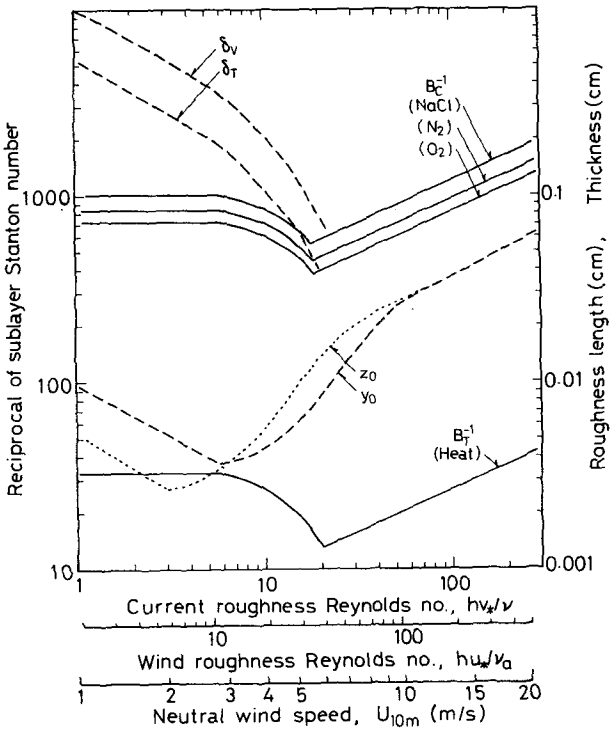


FIG. 2. The hydrodynamic roughness length of current ($y_0$), the thickness of the laminar sublayer for current ($\delta_V$) and that for temperature ($\delta_T$), the reciprocal of the sublayer Stanton number ($B_T^{-1}$) and that of the mass-Stanton number ($B_C^{-1}$) as a function of the current roughness Reynolds number ($hv^*/\nu$). The aerodynamic roughness length of wind ($z_0$) is represented by the dotted line.

$U_{10\,\mathrm{m}}=2.8$ and 11 m s$^{-1}$, respectively, for the current boundary layer; and at $U_{10\,\mathrm{m}}=2$ and 8 m s$^{-1}$, respectively, for the atmospheric boundary layer.

As can be seen from Fig. 2 the roughness lengths for the current are comparable with but larger than those for the wind at $U_{10\,\mathrm{m}} \lesssim 3$ m s$^{-1}$ and vice versa at $3 \lesssim U_{10\,\mathrm{m}} \lesssim 10$ m s$^{-1}$. This interesting result is derived from the assumption of hydrodynamic similarity between the atmospheric and aqueous boundary layers though the geometric roughness $h$ of their interface. Indirect support to the above result will be made later (Fig. 3).

The lines presented in Fig. 2 show sharp changes at $hv^*/\nu \approx 20$, but it is likely that a smooth transition exists from one side to the other. The values of $B^{-1}$ derived from (16) and (17) by using the numerical constants ($b_1$, $p$, $q$, $b_2$, $b_3$) obtained by Owen and Thomson (1963) are shown in this figure. We have not used the constants determined by Yaglom and Kader (1974) and Brutsaert (1975); some differences resulted from the use of different numerical constants will be shown later.

Since the value of $B_C^{-1}$ is one or two order of magnitude larger than that of $f$, the gaseous interchange

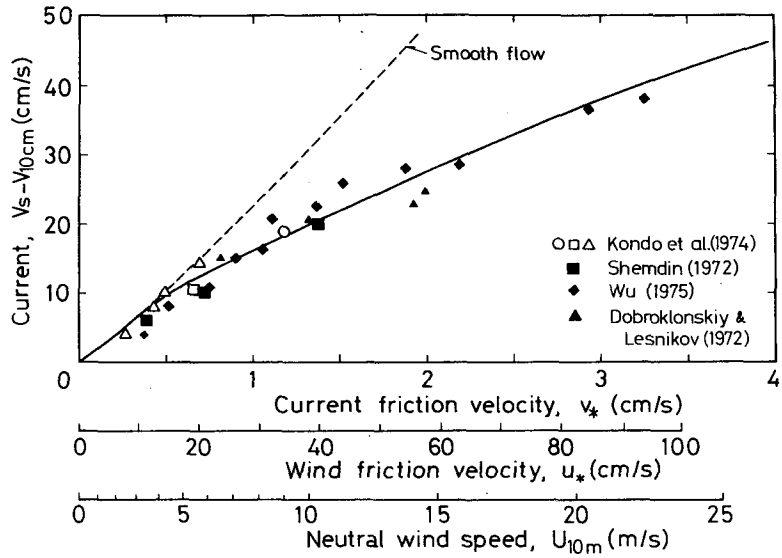


FIG. 3. The current at a depth of $y=10$ cm with respect to the surface as a function of the current friction velocity. Prediction (solid line): $V_s-V_y=(v^*/k)\ln(y/y_0)$; current for smooth surface (dashed line).

between the atmosphere and the ocean is extremely limited in comparison with the momentum exchange.

### *a. Current profile*

Some comparisons between the measurements and the present theoretical results are made. The present theoretical values of the roughness length $y_0$ are comparable with those based on the logarithmic current profile obtained in the tank, ocean and lakes (Kondo *et al.*, 1974), i.e., the measured values are $y_0\approx 2\times10^{-3}$–$5\times10^{-2}$ cm for $v^*=0.2$–$0.8$ cm s$^{-1}$, and $y_0\approx 2\times10^{-2}$ cm for $v^*\approx 1.3$ cm s$^{-1}$.

Fig. 3 shows the current deficit at a depth of 10 cm as a function of $v^*$. The depth of 10 cm is chosen rather arbitrarily, but at this depth there are many available current measurements. The solid line indicates the present theoretical prediction $V_s-V_y=fv^*=(v^*/k)\times\ln(y/y_0)$; the open symbols are from Kondo *et al.* (1974), the solid squares from Shemdin (1972), the small solid squares from Wu (1975), and the solid triangles

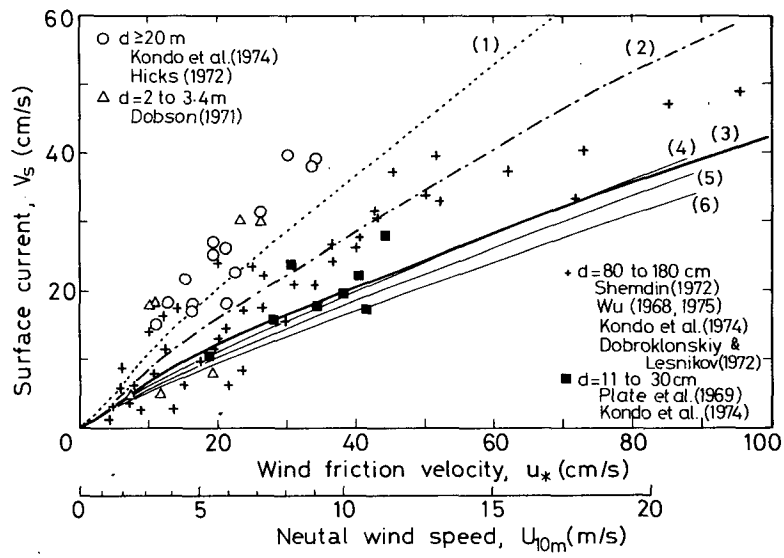


FIG. 4. Surface drift current as a function of wind friction velocity. Prediction of $V_s-V_{10\,m}$ (dotted line); prediction of $V_s-V_{1\,m}$ (dot-dashed line); prediction of $V_s-V_{0.1\,m}$ (heavy solid line); line (4), surface Stokes current for $F=50$ km; line (5), surface Stokes current for $F=1$ km; line (6), surface Stokes current for $F=10$ m.

from Dobroklonskiy and Lesnikov (1972). It can be seen from the figure that the measured currents obtained at different sites and conditions fall in nearly with the present prediction. The measured currents for $v^* \gtrsim 0.5$ cm s$^{-1}$ deviate from the line representing the flow for smooth surface (dashed line).

In Fig. 4 are shown the measured currents $V_s$ at the water surface. The open symbols indicate the data obtained in the ocean (circles are for water depths $d \gtrsim 20$ m; triangles for $d = 2$–3.4 m), the crosses in the shallow lakes and laboratory tanks ($d = 80$–180 cm), and the solid symbols in very shallow channels ($d = 11$–30 cm). Measured results indicate that the current increases with water depth. The present theoretical predictions of $V_s - V_y$ are represented for $y = 10$ m (dotted line 1), for $y = 1$ m (dot-dashed line 2) and for $y = 0.1$ m (solid line 3); and the surface Stokes currents [Eq. (1)] are shown by thin lines for the fetches of $F = 50$ km (line 4), 1 km (line 5) and 10 m (line 6).

From Figs. 3 and 4 it can be seen that the measured current depends strongly on the depth of water, while the shape of the current profile is almost independent of water depth and fetch. The fetch-independent current has also been obtained by Plate *et al.* (1969). The slow current as measured in very shallow channels may be explained by the deterrent force due to bottom friction. In other words, the thickness of the aqueous turbulent boundary layer in the shallow water must be thinner than that in the deep water.

*b. Temperature and mass-concentration profiles*

Regarding the profiles of the temperature and substance-concentration, there are no available data from which comparison can be made with the present theoretical results. The pseudo-thickness of the laminar sublayer for the temperature profile may be defined as

$$\Delta_T = c\rho\alpha(T_s - T)/H, \tag{19}$$

which will result by the use of (3) and (6) as follows:

$$\Delta_T = \alpha\tau_T(y)/v^* = \alpha[f(y) + B_T^{-1}]/v^*. \tag{20}$$

The experimental value of $\Delta_T$ is obtained through Eq. (19) and the theoretical value through (20).

As for the pseudo-thickness of the substance-profile, an analogous definition to the above yields

$$\Delta_C = D\tau_C(y)/v^* = D[f(y) + B_C^{-1}]/v^*. \tag{21}$$

The solid lines of Fig. 5 indicate the pseudo-thickness as a function of $v^*$ (i) for temperature and (ii) for the $N_2$ gas concentration, which are derived from the use of the numerical constants appearing in (16) and (17) by Owen and Thomson (1963). The dot-dashed line and the dotted line indicate the same relations, but the numerical constants used are those obtained by Brutsaert and by Yaglom and Kader, respectively, instead of those by Owen and Thomson. The dashed line, for reference, is that of the flow for a smooth boundary. An interesting feature is that over the range $v^* \gtrsim 2$–3 cm s$^{-1}$ ($hv^*/\nu \gtrsim 200$) the pseudo-thick-

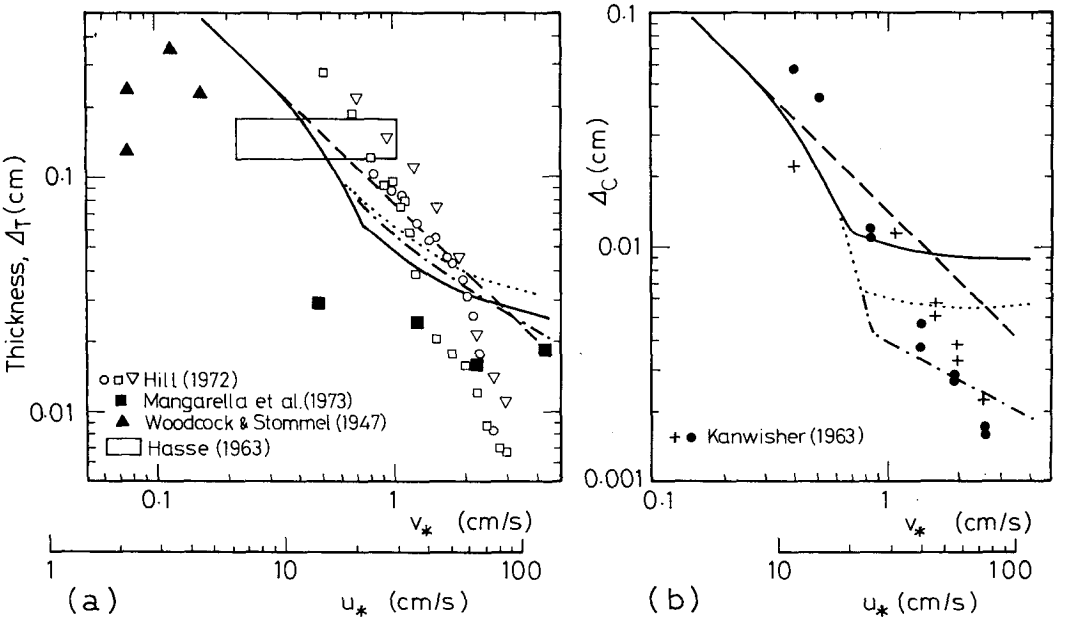


FIG. 5. The pseudo-thickness of the laminar sublayer as a function of the current friction velocity: (a) $\Delta_T$ and (b) $\Delta_C$ for $N_2$ gas concentration. Prediction using the constants by Owen and Thomson (1963) (solid line); prediction using the constants by Yaglom and Kader (1974) (dotted line); prediction using the constants by Brutsaert (1975) (dot-dashed line); for the smooth boundary (dashed line).

ness of the temperature profile for a rough interface is thicker than that for a smooth interface, indicating that heat transfer in an aqueous boundary layer is *reduced* by surface roughness. The same feature is also emphasized by Yaglom and Kader (1974).

The plotted points on Fig. 5a are based on experimental data from Hill (1972) in a small tank (43 cm deep, the free water surface being 40.6 cm wide and 89.5 cm long), and from Mangarella *et al.* (1973) in a tank of about 15 m long and 96 cm deep, and from Woodcock and Stommel (1947) in a pond and Hasse (1963) in the sea.

Since the experiments of Hill were carried out in a small tank, exact comparison should not be made with the present prediction due to the following facts. Mangarella *et al.* (1973) have found that the pseudo-thicknesses of the atmospheric boundary layer above the water surface in a long-fetch channel are much larger than those in a small channel (cf. Fig. 8 of their paper). And Kunishi (1963) has found that in a wind-wave facility the roughness length for wind varies with the fetch and that equilibrium conditions would occur at a fetch greater than several meters, indicating that the smooth-flow regime for wind in a small tank occurs over a wide range of wind speed (or friction velocity) resulting from ill-developed roughness of the waves. On taking the above into consideration, we find that the tendency for measured values of $\Delta_T$ to decrease with increasing $v^*$ is very similar to the behavior of the theoretical value in the smooth to transition regimes, and that the experimental conditions were such that a fully rough regime had not been achieved. From Fig. 5a it can be seen that in the experiment of Hill the current transition takes place at $v^* \approx 1.2$ cm s$^{-1}$ for the smooth to transition regimes, while in the theoretical prediction it takes place at $v^* \approx 0.3$ cm s$^{-1}$; this suggests that the geometric roughness of the water surface in the tank is smaller by a factor of 4 than the roughness employed in the present calculation. This is supported from the fact that the wave initiation (at which the surface geometric roughness may be of the order of $h \approx 0.5$ mm) was visually observed by Hill at the friction velocity $v^* \approx 1.2$ cm s$^{-1}$ ($u^* \approx 35$ cm s$^{-1}$), while the value of $h$ employed in the calculation is about 2 mm at $v^* \approx 0.3$ cm s$^{-1}$. Moreover, experiments showing small values of $\Delta_T$ ($\lesssim 0.01$ cm) at higher wind speeds were probably conducted in conditions beyond the limited application of radiometric temperature measurements of the water surface (cf. McAlister and McLeish, 1969).

According to Hasse (1963), $c\rho(T_s - T_{50\ cm})/H \approx 100$ s cm$^{-1}$ for 34 clear skies observations (where $H = -R - lE - H_a$, $R$ being the net loss of heat emitted by the thermal radiation from the sea surface to the atmosphere, $lE$ the heat due to evaporation and $H_a$ the sensible heat to the atmosphere), resulting in $\Delta_T \approx 0.15$ cm. This is blocked out by the oblong figure and is comparable with the present theoretical prediction.

Experimental determination of the pseudo-thickness of the laminar sublayer is a very difficult task, because the temperature difference $T_s - T$ is only a few tenths of a degree Celcius under ordinary conditions. Though the experimental points may seem to be very scattered owing to these difficulties both the theoretical and experimental values, in general, have the same order of magnitude.

The plotted points in Fig. 5b are based on measurements by Kanwisher (1963) in a small tank (1 m$\times$0.5 m $\times$0.5 m). The trends for the measured values of $\Delta_C$ to decrease with increasing friction velocity are similar to those for the theoretical values in the smooth to transition regime, but the experimental values of $v^*$ at which the change takes place is shifted to the right-hand side of the figure as compared to that for the theoretical value. This would be due to the short fetch and to the consequent non-equilibrium conditions in the experiment as stated previously.

It is noted that the theoretical prediction of $\Delta$ in Fig. 5 corresponds to a depth of $y = 10$ cm, while the experimental values were obtained from data at the depth of several centi- or decimeters, but not just at $y = 10$ cm. However, as the depth changes from $y = 10$ cm to 100 cm (or 1 cm), the theoretical lines are shifted upward (or downward) by only about 10% of the indicated value for $\Delta_T$ and about 1% for $\Delta_C$, respectively.

At the range of $v^* \gtrsim 1.3$ cm s$^{-1}$ which corresponds to about $U_{10\ m} \gtrsim 10$ m s$^{-1}$, the values of $\Delta_C$ as derived from using the numerical constants by Owen and Thomson (solid line) are about three times larger or about one-and-a-half times larger than those derived from using the constants by Brutsaert (dot-dashed line) or by Yaglom and Kader (dotted line), respectively. But we cannot make any decision regarding which expression is preferable. Until more measurements are made at suitable facilities representative of the true open sea, it is difficult to make precise estimates of the global exchange of gaseous substance between the ocean and the atmosphere.

### c. *Turbulent intensity*

According to Speranskaya (1966), in the active layer of the depth of 20 m in a natural reservoir, the vertical turbulent component $w'$ of current fluctuations $(\overline{w'^2})^{\frac{1}{2}} \approx v^*$. Also, Toba *et al.* (1975) have recently showed by use of flow visualization techniques in a wind-wave facility that the current near the water surface is composed of an orbital motion accompanied by some turbulent fluctuations. From their Fig. 4 showing current vectors in which the orbital motion has been subtracted, for $U_{10\ cm} = 8.5$ m s$^{-1}$ ($U_{10\ m} = 16$ m s$^{-1}$), we obtained $(\overline{w'^2})^{\frac{1}{2}} = 2.3$ cm s$^{-1}$ from measurements for $y = 2$–4 cm. On the other hand, the present prediction shows that for $U_{10\ m} = 16$ m s$^{-1}$, the current friction velocity is estimated at $v^* = 2.2$ cm s$^{-1}$, which

yields the ratio of $(w'^2)^{\frac{1}{2}}/v^* = 1.05$. This coincides with the value of $(\overline{w_a'^2})^{\frac{1}{2}}/u^* \approx 1.3$ which is known as the ratio for the atmospheric boundary layer ($w_a'$ is the vertical turbulent component of wind fluctuation in the air layer). Such a similarity is very interesting.

## 5. Conclusions

In the aqueous boundary layer just below the air-water interface, the purely turbulent transport hypothesis has been proposed with hydrodynamic similarity and with the assumption that both the atmospheric and aqueous boundary layers are combined through the identical geometric roughness of their interface. The present similarity hypothesis accounts satisfactorily for the measured current profiles. On the other hand, there are uncertainties in the temperature and substance-concentration profiles due to the lack of available data. It is hoped that more experiments will be performed under long fetch and strong winds so that precise values of the mass-transfer Stanton number can be obtained for large Schmidt numbers ($\nu/D$).

## APPENDIX

### Thickness of the Dynamic Sublayer

It is known that in the atmospheric boundary layer, the logarithmic profiles of wind speed, air temperature, etc., exist within layers of about one-tenth of the dynamic sublayer thickness which is equivalent to the absolute value of the Monin-Obukhov stability length $L$ (Lumley and Panofsky, 1964). By analogy with the above, we can define the length for the aqueous boundary layer having a constant flux as

$$L = -\frac{v^{*3}}{k\frac{g}{\rho}\frac{P}{g}}, \tag{A1}$$

where $P$ is the potential energy flux

$$\frac{P}{g} = \overline{\rho' w'} = -K_p \frac{d\rho}{dy}, \tag{A2}$$

$\rho'$ being the density fluctuation component and $K_p$ the eddy diffusivity for potential energy.

Assuming that $K_p = K_h$ ($K_h$ being the eddy thermal diffusivity) results in

$$L = -\frac{v^{*3}}{k\frac{g}{\rho}\frac{d\rho}{dT}\frac{H}{c\rho}}. \tag{A3}$$

From (A3), if we take the values of $H = 200$ W m$^{-2}$ and $T \approx 20$°C, it is found that $L \approx 60$ m for $v^* = 1.32$ cm s$^{-1}$ (corresponding to $U_{10\,\mathrm{m}} = 10$ m s$^{-1}$) and $L \approx 6$ m for $v^* = 0.60$ cm s$^{-1}$ ($U_{10\,\mathrm{m}} = 4$ m s$^{-1}$). These values of $L$ change slightly in the upper ocean due to the fluctuating chlorinity of sea water.

*Acknowledgments.* The author wishes to express his hearty thanks to Professor Toba and collaborators for providing the original data of their wind-wave experiments and for fruitful discussions.

## REFERENCES

Brutsaert, W., 1975: A theory for local evaporation (or heat transfer) from rough and smooth surfaces at ground level. *Water Resources Res.*, **11**, 543–550.

Dobroklonskiy, S. V., and B. M. Lesnikov, 1972: A laboratory study of the surface layers in drift currents. *Izv. Atmos. Oceanic Phys.*, **8**, 1177–1187.

Dobson, F. W., 1971: Measurements of atmospheric pressure on wind-generated sea waves. *J. Fluid Mech.*, **48**, 91–127.

Hasse, L., 1963: On the cooling of the sea surface by evaporation and heat exchange. *Tellus*, **15**, 363–366.

Hicks, B. B., 1972: Some evaluations of drag and bulk transfer coefficients over water bodies of different sizes. *Boundary-Layer Meteor.*, **3**, 201–213.

Hill, R. H., 1972: Laboratory measurement of heat transfer and thermal structure near an air-water interface. *J. Phys. Oceanogr.*, **2**, 190–198.

Imasato, N., and H. Kunishi, 1971: A note on the energy transfer from wind to waves. *Contr. Geophys. Inst., Kyoto Univ.*, **11**, 71–76.

Kanwisher, J., 1963: On the exchange of gases between the atmosphere and the sea. *Deep-Sea Res.*, **10**, 195–207.

Kondo, J., 1975a: Air-sea bulk transfer coefficients in diabatic conditions. *Boundary-Layer Meteor.*, **9**, 91–112.

——, 1975b: Heat balance of the East China Sea for AMTEX '74. AMTEX Report No. 8, Management Committee for AMTEX, Japan, 12–15.

——, Y. Fujinawa and G. Naito, 1972: Wave-induced wind fluctuation over the sea. *J. Fluid Mech.*, **51**, 751–771.

——, —— and ——, 1973: High-frequency components of ocean waves and their relation to the aerodynamic roughness. *J. Phys. Oceanogr.*, **3**, 197–202.

——, ——, and ——, 1974: Wind-induced current in the uppermost layer of the ocean (in Japanese with English abstract). Rep. Nat. Res. Center Disaster Prevention, Tokyo, No. 8, 67–82.

Kunishi, H., 1963: An experimental study on the generation and growth of wind waves. *Disaster Prevention Res. Inst. Kyoto Univ. Bull.*, No. 61, 1–41.

Lumley, J. L., and H. A. Panofsky, 1964: *The Structure of Atmospheric Turbulence.* Wiley, 239 pp.

Mangarella, P. A., A. J. Chambers, R. L. Street and E. Y. Hsu, 1973: Laboratory studies of evaporation and energy transfer through a wavy air-water interface. *J. Phys. Oceanogr.*, **3**, 93–101.

McAlister, E. D., and W. McLeish, 1969: Heat transfer in the top millimeter of the ocean. *J. Geophys. Res.*, **74**, 3408–3414.

McLeish, W., and G. E. Putland, 1975: Measurements of wind-driven flow profiles in the top millimeter of water. *J. Phys. Oceanogr.*, **5**, 516–518.

Mitsuyasu, H., 1971: On the form of fetch-limited wave spectrum. *Coastal Eng. Japan*, **14**, 7–14.

Owen, P. R., and W. R. Thomson, 1963: Heat transfer across rough surfaces. *J. Fluid Mech.*, **15**, 321–334.

Plate, E. J., P. C. Chang and G. M. Hidy, 1969: Experiments on the generation of small water waves by wind. *J. Fluid Mech.*, **35**, 625–656.

Schlichting, H., 1968: *Boundary Layer Theory*, 6th ed. McGraw-Hill, 747 pp.

Shemdin, O. H., 1972: Wind-generated current and phase speed of wind waves. *J. Phys. Oceanogr.*, **2**, 411–419.

Speranskaya, A. A., 1966: Influence of stability on the characteristics of vertical turbulent exchange in fresh-water reservoir. *Meteor. Gidrol.*, No. 8, 37–41.

Taira, K., 1972: A field study of the development of wind-waves, Part 1. *J. Oceanogr. Soc. Japan*, **28**, 187–202.

Toba, Y., 1972: Local balance in the air-sea boundary processes (1). *J. Oceanogr. Soc. Japan*, **28**, 109–120.

——, M. Tokuda, K. Okuda and S. Kawai, 1975: Forced convection accompanying wind waves. *J. Oceanogr. Soc. Japan*, **31**, 192–198.

Woodcock, A. H., and H. Stommel, 1947: Temperatures observed near the surface of a fresh-water pond at night. *J. Meteor.*, **4**, 102–103.

Wu, J., 1968: Laboratory studies of wind-wave interactions. *J. Fluid Mech.*, **34**, 91–111.

——, 1975: Wind-induced drift currents. *J. Fluid Mech.*, **68**, 49–70.

Yaglom, A. M., and B. A. Kader, 1974: Heat and mass transfer between a rough wall and turbulent fluid flow at high Reynolds and Péclet numbers. *J. Fluid Mech.*, **62**, 601–623.